Control of a Separating Flow over a Turret

Bojan Vukasinovic* and Ari Glezer†
Woodruff School of Mechanical Engineering,
Georgia Institute of Technology, Atlanta, GA 30332-0405

Control of flow separation over a turret comprised of hemisphere on top of a cylindrical base is demonstrated in wind tunnel experiments at Reynolds number $Re_D \approx 800{,}000$. High-frequency actuation ($St_D \approx 15$) is effected using spanwise arrays of individually-addressable synthetic jet actuators and the control effectiveness is characterized using high-resolution particle image velocimetry (PIV) and surface pressure measurements. The present work has demonstrated that high-frequency synthetic jet actuation can lead to substantial separation delay, and that extent of separation delay is directly proportional to both the jet momentum coefficient and the spanwise width of the actuator array. Detailed PIV measurements near the juncture between the hemisphere and the cylinder show that in the presence of nominal actuation there is virtually no recirculating flow within the measurement window down to the level of the juncture between the hemisphere and the cylinder, and suggest that the boundary layer on the surface of the hemisphere is actually attached. However, the pressure distributions show that the static pressure levels off at elevation angle greater than 145°, which may be attributed to 3-D effects. Estimates of the turbulent kinetic energy within the flow downstream of the hemispherical cap show a rather dramatic reduction in TKE in the controlled flow, as the recirculating flow domain is pushed below the hemisphere-cylinder juncture. It is also shown that the presence of a partition plate downstream of this juncture prevents vertical advection of the reduced recirculating flow domain and forces it towards the corner much like in the flow behind a hemispherical shell on a flat plate.

Nomenclature

γ	=	elevation angle
γ_a	=	elevation angle of the actuators
γ_s	=	separation angle
$\Delta\gamma_s$	=	separation delay
ν	=	kinematic viscosity
b_j	=	actuator orifice width
C_μ	=	jet momentum coefficient
D	=	turret diameter
k	=	turbulent kinetic energy
M	=	Mach number
U_i	=	i-component of the velocity
$\overline{U}_i$	=	i-component of the mean velocity
u_i	=	fluctuation of the i-component of the velocity
U_0	=	free stream velocity
U_j	=	average jet velocity
p	=	static pressure
Re_D	=	Reynolds number
St_D	=	Strouhal number

* Research Engineer, AIAA Member.
† Professor, Associate Fellow AIAA.

I. Background

OPTICAL windows that can provide wide (nearly 2π steradian) orientations are typically realized in bluff-body turret configurations comprised of a hemispherical shell on top of a cylindrical base. As shown schematically in Figure 1, such windows are typically plagued by massive, three-dimensional flow separation that is complicated by the formation of both stationary (e.g., trapped, "necklace") vortices, and the nominally time-periodic shedding and advection of large vortical structures downstream of the turret. Therefore, flow separation on these turrets can adversely affect optical transmission due to time-dependent aero-optical distortion and mechanical vibrations of the structure due to the induced unsteady aerodynamic forces. The flow separation off the turret surface is driven by two instability mechanisms namely, a local instability of the separating shear layer and, more importantly, a wake instability that ultimately results in the formation and shedding of large-scale vortical structures. The large-scale wake instability couples with and dominates the initial shear layer instability and feeds back to the separation point, driving the global instability at frequencies that are considerably lower than those of the separating shear layer.

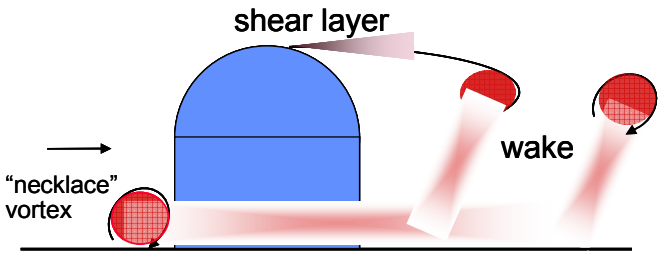

Figure 1. *Illustration of flow separation behind a bluff-body turret.*

Earlier work on separated flows over three-dimensional aircraft turret configurations has been directly motivated by aero optics problems. As noted above, these configurations have been mostly comprised of a cylindrical base with a hemispherical cap, having a flat optical window. The resulting flow field is quite complex as discussed by de Jonckheere, Russel, and Chou[1] and illustrated in Figure 1. The separated flow behind the turret with different flat apertures and the effects of passive control on the optical aberrations were addressed and characterized by Gordeyev, Jumper, Ng, and Cain[2], while the aero-optical characterization of the baseline flow field over a turret configuration was recently investigated by Gordeyev, Hayden, and Jumper[3].

Earlier attempts for controlling the separated flow over a turret exploited the steady suction to modify the wake structure by Purohit, Shang, and Hankey[4] and the addition of aft-mounted fairings and splitter plates by Snyder, Franke, and Masquelier[5]. Purohit et al.[4] showed significant alteration of the wake structure even at low suction levels , while Snyder et al.[5] achieved a reduction of the baseline drag by as much as 55%. However, the addition of fairings obstructs the field of regard downstream of the turret and therefore its utility for aero-optics applications is rather limited. It is noteworthy that the basic configuration of a hemispherical shell on a flat surface has received very little attention, except for atmospheric flows over hemispherical domes[6]. In a numerical investigation of such a flow, Manhart[7] found that Karman-like vortex train is shed from the hemisphere. In these flows however, the thickness of the upstream boundary layer is comparable to the hemisphere radius unlike the flow over an aircraft turret for which the oncoming boundary layer thickness is much smaller than the cylinder height. The effectiveness of direct, high-frequency control ($St_D > 10$) of the separated flow over a hemispherical turret on a flat plate with a thin upstream boundary layer was demonstrated by Vukasinovic et al.[8] at $Re_D = 4 - 7 \times 10^5$. These authors showed that the presence of flow control can substantially reduce the extent of the recirculating domain downstream of the hemisphere with significant reduction in turbulent kinetic energy. The cross stream reduction in the extent of the recirculating domain is limited by the presence of the flat plate.

The present paper focuses on the control of three dimensional separation over a turret comprised of a hemispherical shell on top of a cylinder. Unlike the earlier experiments of Vukasinovic et al.[8], the presence of the cylinder allows for cross stream displacement of the recirculating separated domain in the near wake. The present work draws on earlier investigations of the effectiveness of high-frequency synthetic jet actuation[8] to explore the response of the separated region behind a turret to the fluidic control at $St_D > 10$. The effect of this control approach is twofold. First, virtual surface shaping[9] results in partial suppression and delay of flow separation by local displacement of the baseline flow streamlines and alteration of the streamwise pressure gradient. The ability to eliminate or mitigate separation over optical windows will substantially alleviate unsteady aero optical distortions. Second, even in situations when the separation cannot be significantly delayed, high frequency actuation yields dissipative mechanisms that suppress the natural flow instabilities and thereby the formation and shedding of large-scale vortical structures[10], which substantially contribute to time-dependent aero optical distortions.

II. Experimental Setup and Procedures

The present experiments are conducted in an open-return wind tunnel having a test section that measures 91 cm on the side. A nominal turret (Figure 2*a*) consists of a full sphere that is mounted on top of a 9.5 cm high cylindrical base having the same outer diameter ($D = 30.8$ cm) placed on the bottom wall of the tunnel test section. To assess the effects of a plane surface on the evolution of the separated flow domain downstream of the hemisphere a passive partition plate can be mounted on the downstream face of the sphere-cylinder juncture, as shown schematically in Figure 2*b*. The partition also decouples between the hemisphere and cylinder wakes, which renders a flow over the modified turret qualitatively closer to the flow over a simpler geometry of the hemisphere mounted on a flat surface.

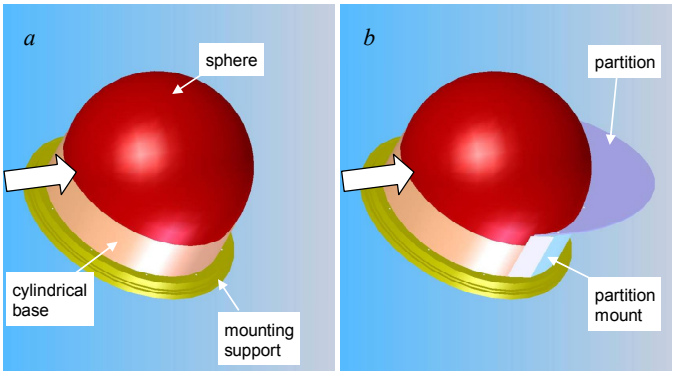

Figure 2. *Schematics of the turret model (a) and with a passive partition (splitter) plate (b).*

Side- and top view projections of turret model are shown in Figure 3 ($R = 15.4$ cm, $H = 9.5$ cm). The model is equipped with two rows of individually-addressable high-frequency synthetic jet actuators that issue normal to the hemisphere surface at average jet velocities up to $U_j = 60$ m/s. The actuators are mounted side by side along the hemispherical arc where each row has eleven actuator modules (flush mounted on the surface). The actuator elevation angle γ_a, relative to the horizon, is adjusted by the sphere rotation, while the sphere azimuthal angle is unchanged. The actuation angle γ_a is defined as the angle of the symmetry axis between the two actuator rows such that the synthetic jets issue at $\gamma_a - 1.9°$ and $\gamma_a + 1.9°$. Each actuator module has two spanwise orifices each measuring 0.38×18.3 mm, 1.9 mm apart. The sphere is also equipped with 64 pressure ports that are arranged in three rows in the free-stream flow direction along the sphere surface in groups of 24, 22, and 18 ports in the central, middle, and outer planes, respectively, as shown in Figure 3*b*. The middle plane cuts through the hemisphere at $z/R = 1/3$, while the outer plane is at $z/R = 2/3$. The static pressure along the hemisphere surface is measured using a dedicated 64-port PSI system.

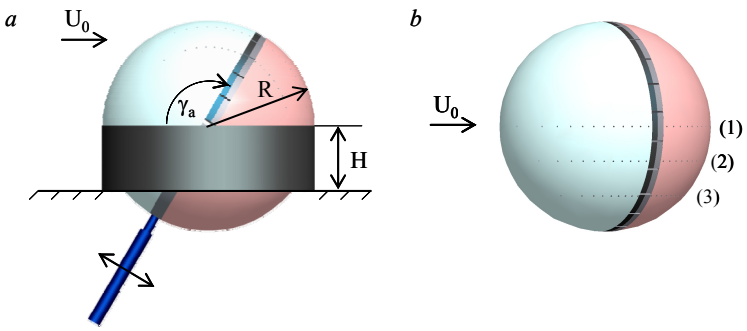

Figure 3. *a) Side-view of the turret model with two actuator rows of adjustable angle γ_a. b) Top-view of the turret model showing three rows of pressure ports along the central (1), middle (2), and outer (3) planes.*

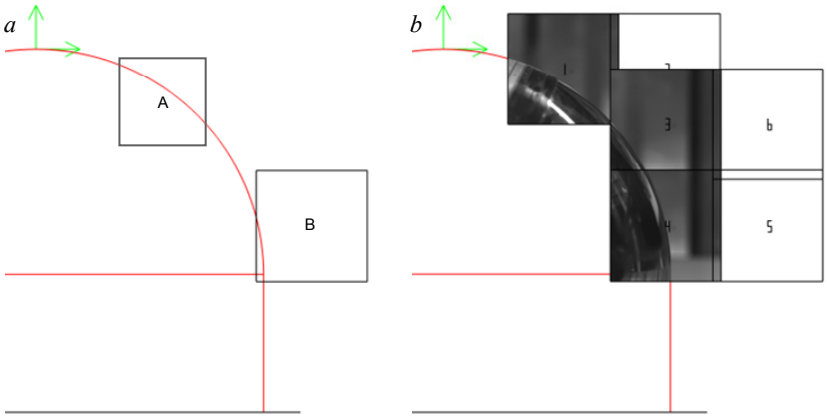

Figure 4. *PIV measurement domains (a) and a composite view of 6 partially overlapping PIV windows (b).*

The flow field over the hemisphere is characterized using PIV measurements within the plane of symmetry (that includes the central 24 pressure ports). The PIV camera is mounted on a two-axis computer-controlled traverse. The effects of the actuation momentum coefficient C_μ. and of the spanwise extent of the actuator array on separation delay are investigated in the two fields of view marked A and B, respectively in Figure 4. The "full" near wake flow field is mapped using six individual, partially overlapping PIV images as shown in Figure 4*b*. Frames 1, 3, and 4 include the snapshots that outline the sphere surface. The two actuators rows are clearly visible in frame 1.

The pressure distributions (in terms of the local elevation angles γ) in the planes $z/R = 1/3$, and 2/3 are projected on the central plane, as shown in Figure 5. Thus, the elevation angle in each plane is represented by the corresponding angle $\gamma \equiv \gamma_c$ in the central plane. Therefore, an angular position γ corresponds to the same streamwise location x in all three planes. The present data are obtained for Reynolds number $Re_D = 800{,}000$ and nominal actuation Strouhal number $St = fD/U_0 = 15.4$. To fix the location of the turbulent boundary layer separation, a 254 μm dia. trip wire is placed across the hemisphere surface at about $\gamma = 30°$, which results in the baseline (tripped) flow separation between $115° < \gamma_s = 120°$. The nominal jet momentum coefficient $C_\mu = \rho U_j^2 A_j/(\rho U_0^2 A_0)$, where A_j is the total jet orifice area and A_0 is frontal projection of the turret, is nominally 0.0098 (down to $C_\mu = 0.0028$ was also used). The actuators' elevation angle γ_a is varied between 90° and 130°. Both rows of actuators are operated in all controlled cases and groups of 3, 7, 9, and 11 actuators are used corresponding to spanwise angular coverage $\beta = 46.2°$, 77°, 107.8°, 138.6°, and 169.4°, respectively.

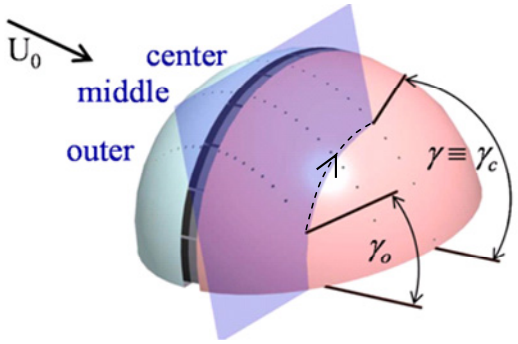

Figure 5. *Schematics of the projection of the outer local angles γ_o to the central angle $\gamma \equiv \gamma_c$.*

III. Control of the Separating Flow Over the Turret

The present flow control strategy has two primary objectives namely to delay separation and to minimize flow fluctuations (and turbulent kinetic energy) downstream of the turret. The influence of several actuation parameters on the actuation effectiveness are investigated including jet momentum coefficient, the relative angular distance between the actuator array and the separation point (in the center plane $z = 0$), and the spanwise extent of the actuator array. For an optimal actuation elevation, the flow field in the near wake (cf. Figure 4*b*) is characterized in the absence and presence of actuation. Finally, the effects of a (passive) solid partition between the hemisphere and cylinder wakes (cf. Figure 2) is assessed and the resulting flow field is compared to the corresponding fields of the nominal turret configuration.

A. Actuator Momentum Coefficient

As the actuation angle is varied within the range $90° < \gamma_a < 130°$, the actuators' momentum coefficients is incremented at the levels $C_\mu \times 10^3 = 2.8$, 4.4, 6.1, 7.9, and 9.8. As expected, the results show a direct relationship between the jet momentum coefficient and the extent of separation delay. For example, static pressure profiles in the three measurement planes for the flow actuated at $\gamma_a = 110°$ ($St = 15.4$) are shown in Figure 6 for a range of jet

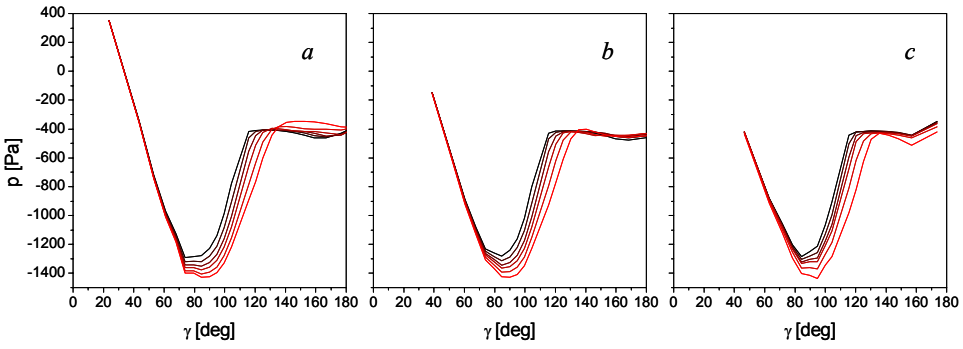

Figure 6. *Static pressure distributions for the baseline (black) and in the presence of actuation ($\gamma_a = 110°$, $St = 15.4$, and $C_\mu \times 10^3 = 2.8$, 4.4, 6.1, 7.9, and 9.8, in the central (a), middle (b), and outer (c) plane. Increasing C_μ levels are marked by increasing red intensity.*

momentum coefficients. These pressure distributions are characterized by an abrupt change in slope on the rear hemisphere surface, which is typically thought of as the onset of separation. For the purpose of using the pressure data to assess the effectiveness of the actuation, the difference in elevation angles $\Delta\gamma_s$ corresponding to the points of abrupt change in the pressure recovery is taken to be the measure of separation delay. However, it is also noted that the high-resolution PIV measurements (Figure 11*f*) suggest that even when the static pressure levels off, the flow along the centerline may not be separated, and that prevailing static pressure may be attributed to 3-D effects. The pressure distributions in Figure 6 indicate that the separation is significantly delayed as the momentum coefficient increases. However, the extent of separation delay decreases from the central to the outer plane. Thus, actuation at highest C_μ results in separation delay of about 25°, 20°, and 17° in the center, middle and outer planes, respectively. The spanwise decrease in actuation effect was reported in the earlier work on a hemispherical turret by Vukasinovic et al.[8], and was attributed to the spanwise change in distance between the actuator location local separation. Separation was fixed across the span just upstream of the actuator array using a trip wire and consequently the spanwise nonuniformity in separation delay was improved but not completely eliminated[8]. The other contributing factors to the spanwise diminution in the actuation effectiveness may be related to the complex unsteady motions that are associated with the separated flow domain and interactions with the necklace vortices.

Figure 7 shows time-averaged velocity and vorticity fields of the separating flow in the center plane $z = 0$ (domain A in Figure 4*a*) in the absence and presence of actuation. Triangle symbol marks the actuation angle. As indicated by the pressure measurements, these data show that the separation point clearly migrates downstream when the jet momentum is increased. At $C_\mu = 0.0061$ (Figure 7*d*), the separation moves outside of the measurement domain, and the flow appears to be fully attached for higher levels of C_μ (cf. Figure 7*f*).

B. Actuator Elevation

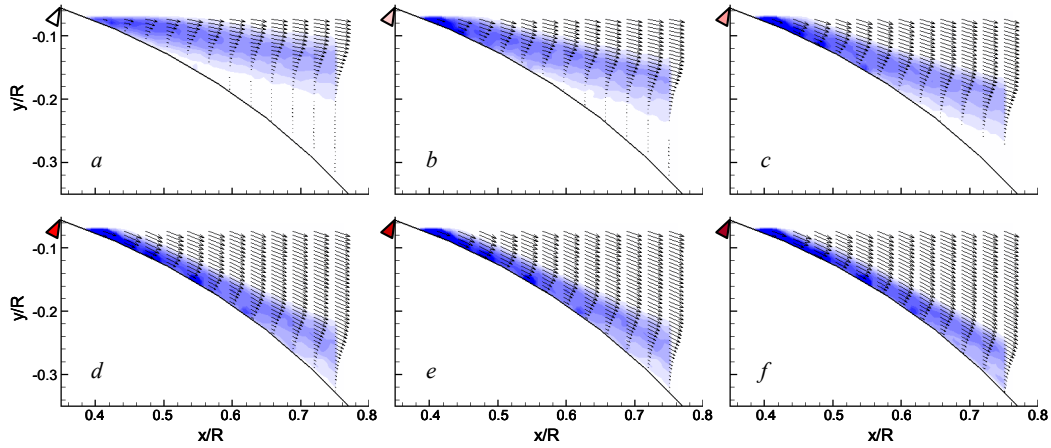

Figure 7. *Equidistant time-averaged cross stream velocity distributions and vorticity raster plots for the baseline (a) and actuated flows at γ_a = 110°, St = 15.4, and $C_\mu \times 10^3$ = 2.8 (b), 4.4 (c), 6.1 (d), 7.9 (e), and 9.8 (f). Vorticity ζ_z (s^{-1}) contour levels: -12000 12000.*

The effect of actuator position relative to the separation line in the unforced flow is investigated when the actuator array is placed 20° and 7° upstream of and 2° downstream of separation. Figure 8 shows static pressure distributions in the three measurement planes as the actuation momentum coefficient is increased. As noted above, the strongest effect in separation delay is achieved in the central plane, and it diminishes in the spanwise direction towards the outer plane. Even when the actuation is applied 20° upstream of separation, the separation point moves downstream by about 18°, 12°, and 8° in the central, middle, and outer planes, respectively. By moving the actuation closer to (7° upstream of) the separation point the separation is delayed by about 26°, 19°, and 16° in the three measurements planes. It is interesting to note that the even better results are achieved when the actuation is applied just downstream (2°) from separation as the separation delay is close to 30° in the center plane.

To further illustrate that once a sufficient C_μ is attained, there is a relatively broad range of actuation angles that result in substantial delay in flow separation, Figure 9 shows pressure distributions in the three measurement planes for the actuation at the maximum C_μ at three actuation angles γ_a = 90°, 120°, and 130°. Along with the pressure distributions for γ_a = 110° (Figure 6), these distributions include two actuation angles upstream and downstream of separation. It is noteworthy that the three cases shown in Figure 9 yield comparable results in the middle plane

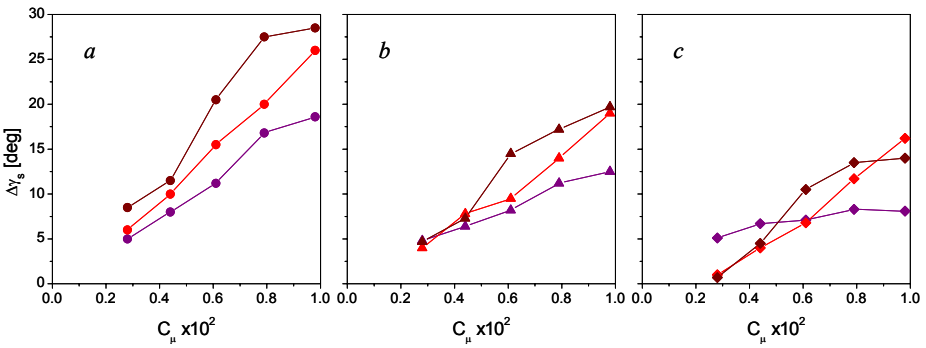

Figure 8. *Variation of separation delay with C_μ in the center (a), middle (b), and outer planes (c), for the relative actuation at 20° (—), and 7° (—) upstream of and 2 ° (—) downstream of separation.*

despite the three-dimensionality of the base flow. Actuation at $\gamma_a = 130°$ is at the furthest local downstream position from separation in the central plane and, consequently, the effect of actuation is different than for the other two cases; the pressure distribution suggests that there is a local attachment of the flow past the actuator location, that is followed by a secondary separation. In contrast to the central plane, the effect of actuation in the outer plane is similar for $\gamma_a = 120°$ and 130°, but weaker for $\gamma_a = 90°$. Again, this is probably a consequence of the relative local position of the actuators because at $\gamma_a = 90°$ the actuators are farthest from the local separation, and therefore their effectiveness is somewhat diminished.

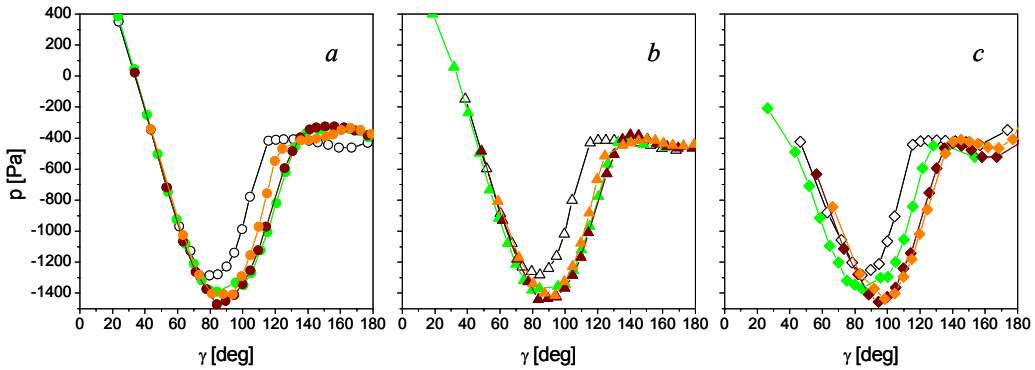

Figure 9. *Static pressure distributions for the baseline (—) and the actuated flows at St = 15.4, $C_\mu = 0.0098$, and $\gamma_a = 90°$ (—), 120° (—), and 130 ° (—), along the central (a), middle (b), and outer (c) planes.*

C. Spanwise Extent of the Actuator Array

The sensitivity of control effectiveness to the spanwise extent of the actuator array is motivated by the limited diameter of typical optical windows over which it is necessary to control the flow. To this end, the number of active actuators in the array is varied symmetrically about the hemisphere's apex namely, arrays of 3, 5, 7, 9 and 11 actuators corresponding to spanwise angular coverage $\beta = 46.2°$, 77°, 107.8°, 138.6°, and 169.4°. The actuation is applied 7° upstream of separation. For the full, 11 actuator array $C_\mu = 0.0098$ and it proportionally decreases with the number of active actuators. Static pressure distributions in the three measurement planes are shown in Figure 10. Pressure distributions in the central plane (Figure 10*a*) clearly indicate that there is a direct proportional relationship between the spanwise extent of actuation and separation delay in the plane of symmetry. Even with only three active actuators there is a localized separation delay of about $\Delta\gamma_s = 8°$. As the spanwise extent of array increases, there a progressive increase in separation delay up to about $\Delta\gamma_s = 25°$ when all actuation modules are active. Similar dependence of the spanwise extent of actuation and separation delay is seen in pressure distributions in the middle plane (Figure 10*b*). At this plane, there is a marginal effect when only the top three actuators are active while the middle plane is barely within the active actuation span. The effect of the actuation is sensed in the outer plane only when the number of active actuators in the array is over seven ($\beta = 107.8°$, Figure 10*c*). As the actuation span increases to $\beta = 138.6°$ and 169.4°, a substantial delay in separation is measured, up to about $\Delta\gamma_s = 17°$ when all actuators are active.

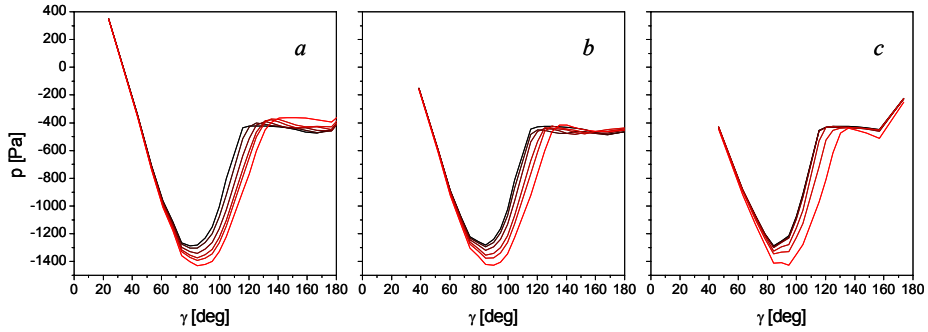

Figure 10. *Static pressure distributions for the baseline (black) and the flows actuated at γ_a = 110°, C_μ = 0.0098, St = 15.4, and β = 46.2°, 77°, 107.8°, 138.6°, and 169.4°, along the center (a), middle (b), and outer (c) planes. The increase in C_μ is marked by increased red intensity.*

The changes induced by the actuation in the structure of the recirculating flow domain immediately downstream of the turret are investigated using PIV measurements within field of view B in Figure 4*a*. Figure 11 shows distributions of the mean vorticity and velocity fields for the baseline flow and in the presence of actuation using the five spanwise array configurations described above. The baseline flow (Figure 11*a*) is evidently fully separated within the measurement domain and the center of the recirculating flow (denoted $x_C^* = x_C/R$, $y_C^* = y_C/R$) is clearly outside of the measurement domain ($x_C^* > 1.5$). As the center three actuators in the array are activated (Figure 11*b*), the center of recirculation is still outside of the measurement domain, but is pushed downward ($y_C^* < -0.7$) towards the hemisphere as the extent of the separated domain decreases and, as can be seen at the top right, the outer flow begins to bend towards the turret. The center of recirculation becomes more visible when the center five and seven actuators are active [x_C^* and y_C^* in Figures 11*c* and *d* are (1.4, -0.8) and (1.3, -0.97), respectively], as the recirculating flow domain begins to diminish and moves closer to the turret surface. When nine actuators are active (Figure 11*e*), the center of the recirculation is pushed below the lower edge of the field of view which is at the level of the juncture between the hemisphere and the cylinder (at about $x_C^* = 1.2$). These changes are accompanied by a significant reduction in the strength of the negative (CCW) vorticity concentration within the boundary layer on the surface of the hemispehere and the separation point is clearly visible near the top edge of the surface). When the full actuator array is active (Figure 11f), *there is virtually no recirculating flow within the measurement window down to the level of the juncture between the hemisphere and the cylinder and the boundary layer on the surface of the*

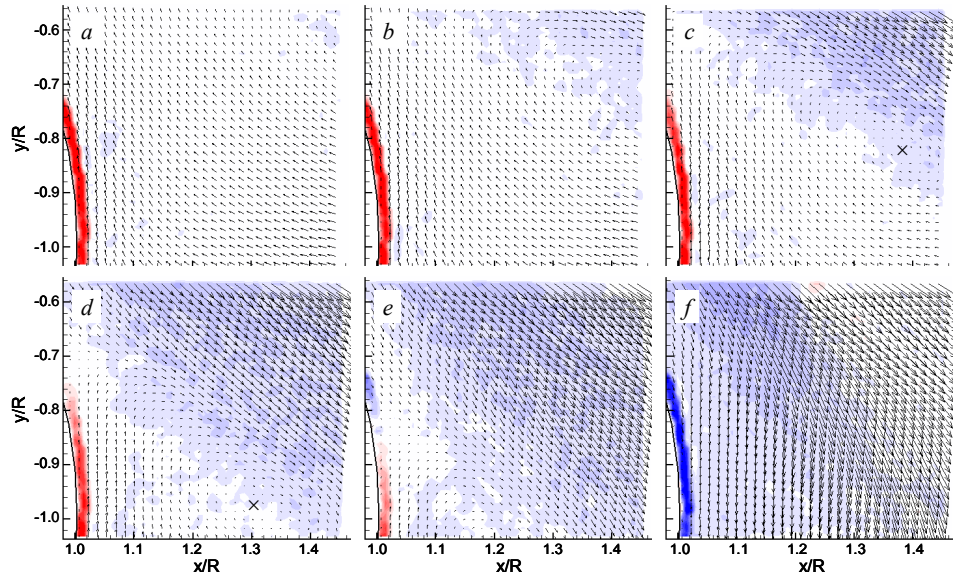

Figure 11. *Time-averaged velocity and vorticity distributions for the baseline (a) and in the presence of actuation (γ_a = 110°, C_μ = 0.0098) for β = 46.2° (b), 77° (c), 107.8° (d), 138.6° (e), and 169.4° (f). Vorticity ζ_z (s^{-1}) contour levels: -4000 4000. Symbol × marks the center of recirculation.*

hemisphere appears completely attached. This finding is remarkable because the pressure distribution (cf. Figure 10*a*) suggests that the static pressure levels off at $\gamma > 145°$ indicating either separation or a closed recirculation bubble. By examining the velocity profile at $x/R = 1$ in the corresponding full-filed measurements (Figure 12*b*), it appears that the mean velocity is indeed of very small magnitude, having no recirculating component. This may suggest that the pressure distribution is affected by the three-dimensional changes in the flow near the base of the hemisphere and does not necessarily indicate the presence of reversed flow.

These data indicate that despite the three-dimensional separation it is possible to utilize limited spanwise actuation to achieve partial flow attachment over segments of the hemispherical surface that would include an optical window. Furthermore, in the vicinity of the center plane flow attachment appears to be complete.

D. Active Dissipation of Flow Fluctuations

A major objective of the present work is to demonstrate that high-frequency flow control can lead to the suppression of the large-scale turbulent motions that are formed by fundamental flow instabilities once the flow separates off the turret surface. These velocity fluctuations can strongly contribute to optical aberrations through the field. While controlled suppression of flow separation can obviously eliminate the formation of the near wake instabilities that result in aero optical distortions, full attachment is not always possible owing to the three-dimensional nature of the base flow. Earlier work[8] has demonstrated that even in the absence of full reattachment, high-frequency flow control can lead to significant suppression of the flow instabilities of the separated flow and therefore hold the potential for improving aero-optical transmission even in the separated flow.

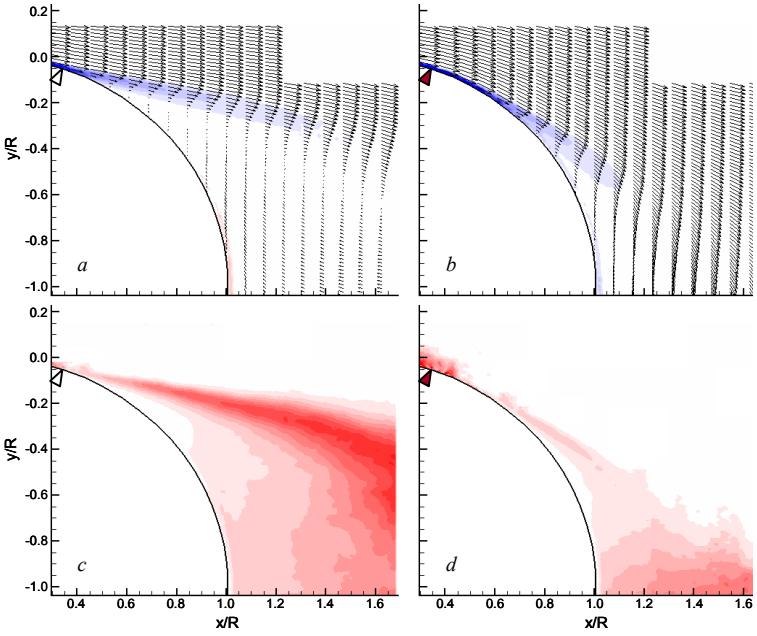

Figure 12. *Time-averaged vorticity and velocity distributions (a, b) and concentrations of turbulent kinetic energy k (c, d) for the baseline (a, c), and actuated (b, d) flows. (γ_a = 110°, C_μ = 0.0098). ζ_z (s^{-1}): -15000 15000. k (m^2/s^2): -100 100.*

To estimate the levels of flow fluctuations in the absence and presence of flow control, the full-field PIV measurements are taken over six partially-overlapping windows, as shown in Figure 4*b*. The flow fluctuations are characterized by a 2-D estimate of the turbulent kinetic energy $k = \overline{u^2}/2 + \overline{v^2}/2$, which is extracted from the ensembles of PIV data. The full-field mean vorticity raster plots with overlaid equidistant mean velocity profiles are shown in Figures 12*a* and *b*, for the baseline and actuated flow at Re_D = 800,000. Actuation is applied at $C_\mu = 0.0098$ and $\gamma_a = 110°$ ($St = 15.4$). In the absence of flow control, the center plane of the near wake is clearly dominated by a large recirculating zone (Figure 12*a*) with the center of recirculation at $x_C^* = 1.6$ and $y_C^* = -0.6$. As noted in connection with Figure 11*f*, the application of flow control (Figure 12*b*) is accompanied by a significant delay of separation and based on vorticity concentrations in the hemisphere's boundary layer, the flow in the center plane appears to be attached while the recirculating flow domain is radically reduced and displaced downward, towards the cylindrical base surface. These changes in the flow result in significant alteration of the turbulent kinetic energy as shown in the raster plots in Figures 12*c* and *d* for the baseline and controlled flows, respectively. As the baseline flow separates, high levels of TKE are apparent to the separating shear layer and within the high-speed edge of the near wake. In addition to the significant delay in separation, it is remarkable that the TKE is strongly diminished in the separating shear layer and within the reduced separation bubble in the near wake of the turret (Figure 12*d*). So besides the spatial shift of the separated flow and the spanwise increase in the extent of attached flow, it is significant that the peak TKE levels within the measurement domain are suppressed by about 40%.

E. Modified Turret Geometry

The last segment of the current study focuses on passive modification of the nominal turret geometry by the addition of a partition plate (Figure 2*b*). This change in geometry is motivated by earlier studies of Vukasinovic et al.[8] of the flow over a surface-mounted hemispherical shell, where actuation resulted in a relatively compact recirculating domain ensued behind the hemisphere due to the juncture between the hemisphere and the support surface. It is anticipated that the addition of the partition may lead to decoupling between the hemisphere and cylinder's wakes.

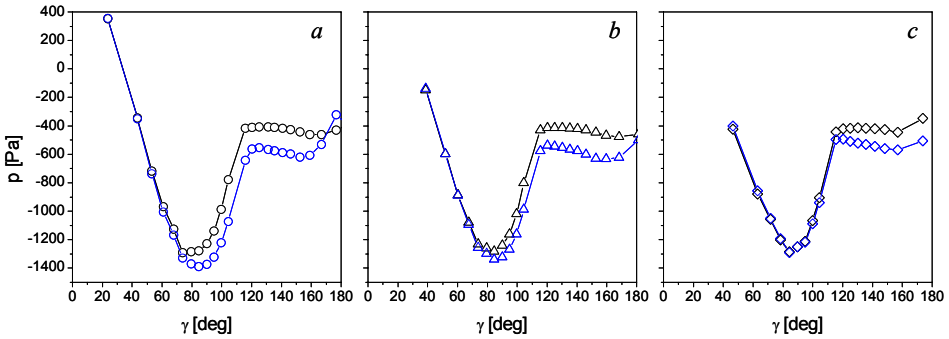

Figure 13. *Static pressure distributions for the baseline flow ($Re_D = 8 \times 10^5$) with (▬) and without (▬) the partition, in the center (a), middle (b), and outer (c) planes.*

Pressure distributions in the three measurement planes for the baseline flow (Re_D = 800,000) with and without the partition plate are shown in Figure 13. These data show that in the outer plane (Figure 13c) there is no significant difference between the two distributions up to the separation point. Although there is no change in separation location, the outer flow over the modified geometry accelerates more downstream from separation, while it is apparently being pulled towards the surface. This acceleration is also apparent in the center and middle planes and begins at the apex well upstream of separation and results in lower static pressure in the near wake which is clearly supported by the partition. However, the separation line seems to be unchanged in the middle plane and results in only a small delay in separation in the center plane. It should be also noted that the static pressure increases towards the edge of the hemisphere ($\gamma = 180^o$), which is associated with the proximity of the recirculating bubble that now forms at the juncture between the hemispherical surface and the splitter plate.

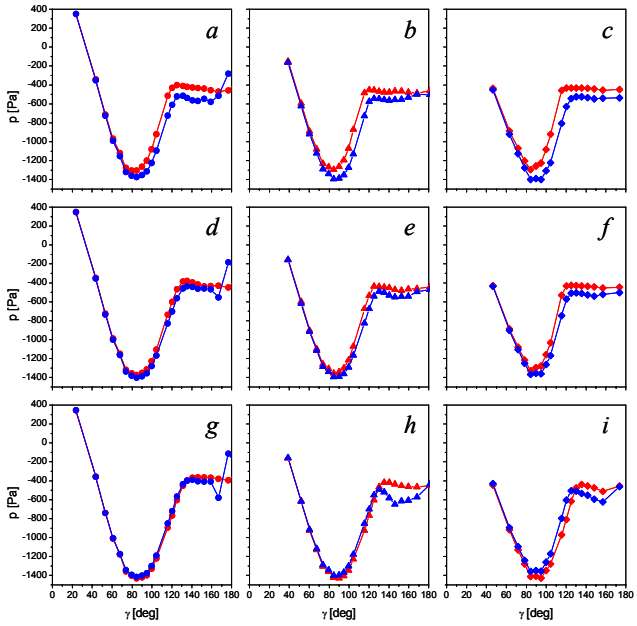

Figure 14. *Static pressure distributions for spanwise-varying actuation (γ_a = 110°, St = 15.4, C_μ = 0.0098), and β = 46.2° (a, b, c), 107.8° (d, e, f), and 169.4° (g, h, i), with (▬) and without (▬) the partition, in the center (a, d, g), middle (b, e, h), and outer (c, f, i) planes.*

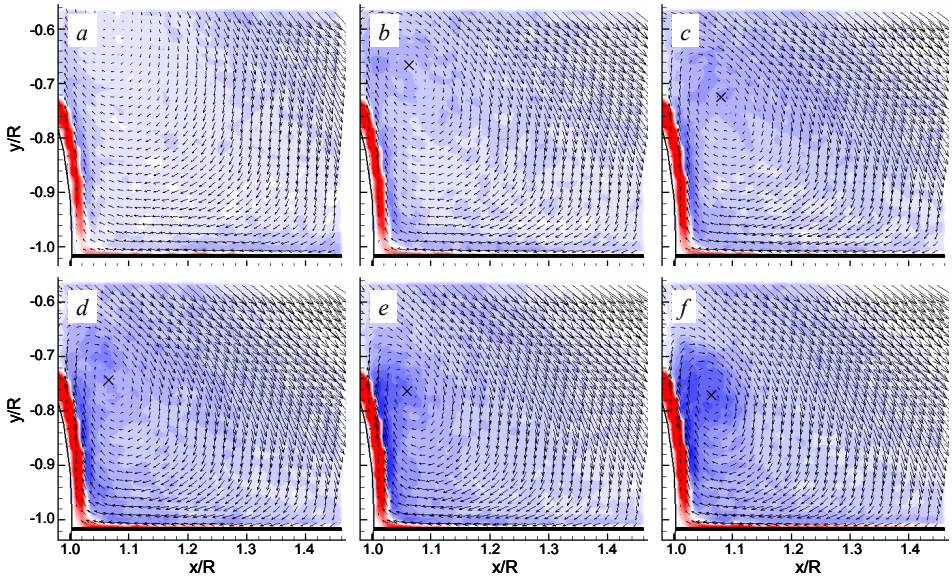

Figure 15. *Time-averaged velocity and vorticity distributions for the baseline (a) and actuated (γ_a = 110°, St = 15.4) flows in the presence of the partition β = 46.2° (b), 77° (c), 107.8° (d), 138.6° (e), and 169.4° (f). Vorticity contour levels are the same as in Fig.11. Symbol × marks the center of recirculation.*

Similar to the measurements in Section III.C, the effect of the spanwise extent of actuation is also investigated for the modified turret geometry. Comparison of three actuation cases at γ_a = 110° (C_μ = 0.0098) using the center three, seven , and eleven actuators active is shown in Figure 14 for the basic and modified turret geometries. It is noteworthy that the presence of the partition leads to enhancement of the actuation effectiveness (as measured by the extent of the attached flow) when the actuation is spanwise-limited. However, these differences become less pronounced as the number of the actuators is increased. When the entire array is used, (Figures 15*g-i*) it appears that the flow attachment is better over the nominal turret geometry, especially in the two off-center planes.

The effect of spanwise extent of actuation over the modified turret is also characterized by PIV measurements within the field B shown in Figure 4*a*. Figure 15 shows the time-averaged vorticity and velocity fields for the baseline flow and with five spanwise actuator configurations. The baseline flow (Figure 15*a*) is characterized by the existence of a recirculating bubble that is bounded from below by the partition and whose center is approximately at mid-height of the hemisphere and close to the surface at $x_C^* \approx 1.05$. When the center three and five actuators are activated (Figures 15*b* and c), the recirculation moves

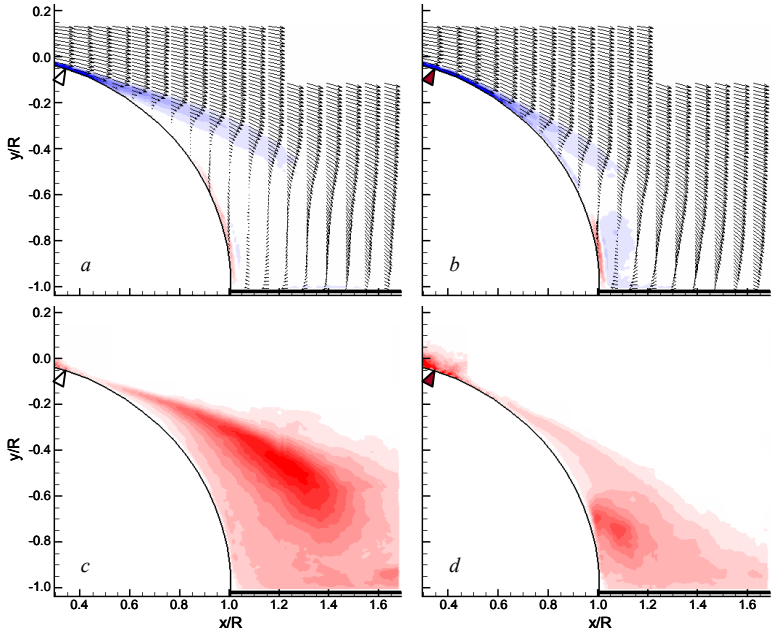

Figure 16. *Time-averaged vorticity and velocity distributions (a, b) and raster plots of turbulent kinetic energy k (c, d) in the presence of the partition for the baseline (a, c), and the actuated flows (b, d, γ_a = 110°, St = 15.4, C_μ = 0.0098). Vorticity and turbulent kinetic energy contour levels are the same as in Fig.12.*

predominantly downward to $y_C^* \approx -0.68$. As the number of actuators and the array's spanwise extent increase, the center of recirculation is not displaced any further (Figures 15*d-f*), but the recirculating CW vortex intensifies. Note that the reattachment on the surface of the partition is $0.4 - 0.5R$ downstream from the hemisphere surface, which is similar to the corresponding findings of Vukasinovic et al.[8] on a surface-mounted hemispherical shell.

Finally, full-field mean vorticity raster plots with overlaid equidistant mean velocity profiles are shown in Figures 16*a* and *b* in the presence and absence of actuation. Comparison of Figures 12*a* and 16*a*, shows that the addition of the partition to the baseline flow reduces the extent of the recirculating domain even though the separation point itself is only marginally changed. Note also that that the center of recirculation moves closer to the surface as a result of the partition. Once the actuation is active (Figure 16*b*), separation is delayed, the circulating bubble is pushed towards the juncture between the surfaces and its size is significantly reduced. While actuation also leads to a reduction in the magnitude of the turbulent kinetic energy k within the recirculating flow (compare Figure 16*c* and *d*), the trapped vorticity is bounded by the presence of the partition and cannot move below its surface as in the case of the unbounded flow.

IV. Conclusions

Separation control of the flow over a turret comprised of hemisphere on top of a cylindrical base is investigated experimentally at Reynolds number Re_D = 800,000. Actuation is applied by a spanwise array of individually-controlled synthetic jet actuators that issue normal to the surface and are operated at a frequency at least an order of magnitude higher than the unstable frequencies of the near wake baseline flow (St_D = 15.4). The control effectiveness is characterized using high-resolution particle image velocimetry (PIV), and surface pressure measurements.

The effectiveness of the actuation for the suppression of optical aberrations through the near wake of the turret is measured by separation delay and reduction of flow fluctuations within the near wake. The effectiveness is characterized in terms of the actuators momentum coefficient, relative distance between the actuator array and the separation line, and the spanwise extent of actuator array. It is found that the extent of streamwise delay in separation is proportional to the magnitude of the actuation momentum coefficient, yielding a nearly 30° increase based on static pressure measurements at the center plane of the hemisphere for $C_\mu = 0.0098$ (scaled to the hemisphere). The control effectiveness in the current configuration is somewhat reduced towards the spanwise edges of the hemisphere owing to three dimensional effects and variation in the distances between the actuation and separation line. While optimal control appears to be achieved when the actuation is applied immediately upstream or downstream from of separation, it is also demonstrated that substantial separation delay can be achieved when actuation is applied over a wide range of angles so that control authority is fairly robust with respect to the relative distance to the separation point. It is also demonstrated that separation delay in the central plane of the turret is affected by the spanwise extent of the actuator array which also increases the spanwise extent of the attached flow domain.

The present work has demonstrated that high-frequency synthetic jet actuation can lead to substantial separation delay. Detailed PIV measurements near the juncture between the hemisphere and the cylinder show that in the presence of nominal actuation *there is virtually no recirculating flow within the measurement window down to the level of the juncture between the hemisphere and the cylinder, and suggest that the boundary layer on the surface of the hemisphere is actually attached.* This finding is remarkable because the pressure distribution (cf. Figure 10*a*) suggests that the static pressure levels off at $\gamma > 145°$. It is suggested that the pressure distribution may be affected by the global three-dimensional changes in the flow near the base of the hemisphere and hence may not necessarily indicative of the presence of localized reversed flow. The actuation also has a profound effect on the magnitude of flow fluctuations within the near wake as may be measured by (estimated) concentrations of turbulent kinetic energy. The present measurements show that high-frequency, dissipative actuation can lead to significant suppression of flow fluctuations within the near wake and therefore to potential improvement in aero optical aberrations. It is also shown that the addition of a horizontal partition at the hemisphere-cylinder juncture (to mimic a hemispherical shell on the flat surface) significantly alters the base flow and prevents the complete migration of the hemisphere's separated flow domain towards the cylinders wake.

Acknowledgment

This work has been supported by the Air Force Research Laboratory and the Boeing Company.

References

[1]de Jonckheere, R., Russell, J. J., and Chou, D. C., "High subsonic flowfield measurements and turbulent flow analysis around a turret proturberance", *AIAA Paper* 82-0057, 1982.

[2]Gordeyev, S., Jumper, E. J., Ng, T. T., and Cain, A. B., "The optical environment of a cylindrical turret with a flat window and the impact of passive control devices", *AIAA Paper* 2005-4657, 2005.

[3]Gordeyev, S., Hayden, T. E., and Jumper, E. J., "Aero-optical and flow measurements over a flat-windowed turret", AIAA J., Vol. 45, 2007, pp. 347-357.

[4]Purhoit, S. C., Shang, J. S., and Hankey, W. L., "Effect of suction on the wake structure of a three-dimensional turret", *AIAA Paper* 83-1738, 1983.

[5]Snyder, C. H., Franke, M. E., and Masquelier, M. L., "Wind-tunnel tests of an aircraft turret model", *J. Aircraft*, Vol. 37, 2000, pp. 368-376.

[6]Toy, N., Moss, W. D., and Savory, E., "Wind tunnel studies on a dome in turbulent boundary layers", *J. Wind Eng. Ind. Aerodynamics*, Vol. 11, 1983, pp. 201-212.

[7]Manhart, M., "Vortex shedding from a hemisphere in a turbulent boundary layer", *Theoret. Comput. Fluid Dynamics*, Vol. 12, 1998, pp. 1–28.

[8]Vukasinovic, B., Brzozowski, D., Glezer, A., Bower, W., and Kibens, V, "Separation control over a surface-mounted hemispherical shell", *AIAA Paper 2005-4878*, 2005.

[9]Honohan, A. M., "The interaction of synthetic jets with cross flow and the modification of aerodynamic surfaces," *Ph.D. Dissertation*, Georgia Institute of Technology, Atlanta, GA, 2003.

[10]Vukasinovic, B., and Glezer, A., "Transitory fluidic control of turbulent shear flows*", AIAA Paper 2006-3227*, 2006.

[11]Smith, B.L. and Glezer, A. "Jet vectoring using synthetic jets", *J. Fluid Mech*., Vol. 458, 2002, pp. 1-34.